FINAL TECHNICAL REPORT

Award Number: **04HQGR0029**
Title: "FURTHER INVESTIGATION OF NEAR-FAULT PULSES AND THEIR CAUSATIVE RELATION TO RUPTURE PROCESSES"

Author: Apostolos S. Papageorgiou, Ph.D.
University at Buffalo
Department of Civil, Structural & Environmental Engineering
Ketter Hall
Box 604300
Buffalo, NY 14260-4300
Phone: (716) 645-2114 x2416; Fax: (716) 645-3733
E-mail: papaga@eng.buffalo.edu

Current address:
University of Patras
Department of Civil Engineering
265 00 Patras, Greece
Phone: +30 (2610) 996-562
E-mail address: papaga@upatras.gr

TECHNICAL ABSTRACT

Near-fault ground velocities generated by earthquakes are characterized by a pulse of intermediate period and intense amplitude.

We investigated the *waveform* of the near-fault pulses and relate it to the causative rupture processes (i.e., the *slip* and *stress* distribution on the fault plane). One of the important conclusions / observations is that for smaller earthquakes (such as the 1979 Imperial Valley earthquake), the area of the fault that contributes to the formation of the near-fault pulse encompasses more than one "*patches*" of significant moment release (*subevents*). This observation should be contrasted with what is observed for the rupture of a major event (such as the 1985 Michoacan earthquake) which encompasses an individual "patch" of significant moment release (subevent). This explains why a dislocation model with average properties (i.e., average slip, rise time, etc) reproduces reasonably well near-fault motions for events such as the 1979 Imperial Valley earthquake, while a crack model would be necessary to model the near-fault motions of a mega-thrust event such as the 1985 Michoacan earthquake.

We investigated the rotational motions [i.e., torsion (= rotation about a vertical axis) and rocking (= rotation about a horizontal axis)] associated with the near-fault intense velocity pulses of earthquake ground motion. We concluded that the analytical model that was used for the representation of the coherent (long-period) component of the near-fault ground motions proposed by Mavroeidis and Papageorgiou (2003) may be used to approximate the torsional component of the near-fault ground motion.

We investigated the response of simple models of structures (such as buildings and towers of cable-supported bridges) to near-fault translational and rotational motions. Based on our investigations we conclude that the accidental eccentricity considered by the current provisions of the building code is adequate to account for the rotational (torsion) motions about a vertical axis induced by the near-fault earthquake displacement field.

NON-TECHNICAL ABSTRACT

Near-fault ground velocities generated by earthquakes are characterized by a pulse of intermediate period and intense amplitude.

We investigate how the stress-drop and slip distribution on the fault plane (during the rupture process) that generate an earthquake are related to the above mentioned velocity pulses. From analyses of well recorded past events we observe that for smaller earthquakes the area of the fault that contributes to the formation of the near-fault pulse encompasses more than one "*patches*" of significant seismic moment release (*subevents*). This observation should be contrasted with what is observed for the rupture of a major event which encompasses an individual "patch" of significant moment release (subevent).

We investigated the rotational motions [i.e., torsion (= rotation about a vertical axis) and rocking (= rotation about a horizontal axis)] associated with the near-fault intense velocity pulses of earthquake ground motion. We concluded that the analytical model that was used for the representation of the coherent (long-period) component of the near-fault ground motions proposed by Mavroeidis and Papageorgiou (2003) may be used to approximate the torsional component of the near-fault ground motion.

We investigated the response of simple models of structures (such as buildings and towers of cable-supported bridges) to near-fault translational and rotational motions. Based on our investigations we conclude that the accidental eccentricity considered by the current provisions of the building code is adequate to account for the rotational (torsion) motions about a vertical axis induced by the near-fault earthquake displacement field.

MAIN BODY OF THE REPORT:

Code provisions have historically been developed based on recorded ground motions not sufficiently close to the causative fault. Thus, the effect of the impulsive character of the near-fault ground motions on the elastic and inelastic performance of conventional, non-conventional (e.g., base-isolated) and special (e.g., long-span bridges) structures has recently received much attention and has become a significant concern for reliable aseismic structural design. The purpose of the investigation is to assess the adequacy of current building code provisions and to contribute (if necessary) to their improvement.

In order to effectively investigate the structural response to near-fault ground motions, the ground motion input should be properly represented and parameterized in terms of simple, yet effective, analytical models whose input parameters have an unambiguous physical interpretation and scale, to the extend possible, with earthquake magnitude. Such a model, that successfully captures the impulsive character of near-fault velocity pulses both qualitatively as well as quantitatively, has been proposed by Mavroeidis and Papageorgiou (2003). The model consists of a very simple mathematical expression. The most important parameters of the model are the "*pulse duration*" T_P and the "*amplitude*" A of the pulse.

With the research project that we completed, we attempted to build on the above accomplishments of our work on near-fault motions. The aim was to accomplish the following tasks:

> Task 1: Investigate the *waveform* of the near-fault pulses and relate it to the causative rupture processes (i.e., the *slip* and *stress* distribution on the fault plane).
> Task 2: Investigate the rotational motions [i.e., *torsion* (= rotation about a *vertical* axis) and *rocking* (= rotation about a *horizontal* axis)] associated with the near-fault intense velocity pulses of earthquake ground motion, and propose a simple mathematical model to describe them, that can be readily used by engineers for earthquake analysis and design of structures.
> Task 3: Investigate the response of simple models of structures (such as buildings and towers of cable-supported bridges) to near-fault translational and rotational motions, perform exploratory parametric analyses to discern the sensitivity of the structural response to various key parameters of the input (e.g., "*pulse duration*" T_P, "*phase velocity*" c, etc), and assess the adequacy of existing building code provisions to account for earthquake motions in the near-fault region.

Task 1:

In our previous work on near-fault motions, we proposed a very simple mathematical expression to describe near-fault velocity pulses (Mavroeidis and Papageorgiou 2003). The mathematical expression for the velocity pulse $v(t)$ is

$$v(t)=\begin{cases} A\frac{1}{2}\left[1+\cos\left(\frac{2\pi f_P}{\gamma}(t-t_0)\right)\right]\cos\left[2\pi f_P(t-t_0)+\nu\right], & t_0-\frac{\gamma}{2f_P}\le t\le t_0+\frac{\gamma}{2f_P} \quad \text{with} \quad \gamma>1 \\ 0, \quad \textit{otherwise} \end{cases} \qquad (1)$$

Parameter A controls the amplitude of the signal, f_P is the frequency of the amplitude-modulated harmonic (or the prevailing frequency of the signal; "*pulse duration*" T_P is related to f_P as $T_P = 1/f_P$), ν is the phase of the amplitude-modulated harmonic (i.e., $\nu = 0$ and $\nu = \pm\pi/2$ define

symmetric and anti-symmetric signals, respectively), γ is a parameter that defines the oscillatory character (i.e., zero-crossings) of the signal (i.e., for small γ the signal approaches a delta-like pulse; as γ increases the number of zero-crossings increases), and t_0 specifies the "*epoch*" of the envelope's peak.

By calibrating the model using the database of virtually all of the near-fault ground motions recorded globally so far, Mavroeidis and Papageorgiou (2002a,b; 2003) found that the "*pulse amplitude*" A is roughly constant, independent of magnitude, having an average value of $\sim 100 cm/s$, while the "pulse duration" T_P scales with moment magnitude M_W as follows: $\log T_p = 0.5 M_W - 2.9$. Furthermore, Mavroeidis and Papageorgiou (2004) found that the "pulse duration" T_P is related to the "*rise time*" τ as follows: $\tau \approx 0.5 T_p$. The "epoch" t_0 of the signal represents a mere shift of the origin of the time axis and therefore has no physical significance. For the other two parameters of the signal, ν and γ, Mavroeidis and Papageorgiou (2002c) have not observed any obvious correlation with magnitude. The parameters ν and γ control the waveform of the pulse. It is reasonable to believe that parameters ν and γ are related to the details of the slip and stress distribution on the fault plane, and we would like to investigate this relation.

In order to investigate the relation of the near-fault velocity pulse waveform to the slip and stress spatio-temporal history over the fault plane we proposed to investigate events that produced near-fault strong motion recordings and for which reliable tomographic images of the evolution of slip have been inferred by inversion. In order to infer the stress distribution on the fault plane, we followed the method that Bouchon (1997) proposed. Specifically, Bouchon (1997) implemented the "*Discrete Wave-number Method*" to compute the evolution of stress changes on the fault plane. This is the method that originally Bouchon and Aki (1977) and Bouchon (1979) had proposed to compute the wave-field generated by a seismic source (such as a shear fault) in layered homogeneous isotropic elastic half-space. Using this method Bouchon (1997) investigated the evolution of stress on the fault plan for the 1979 Imperial Valley 1984 Morgan Hill, 1989 Loma Prieta, and 1994 Northridge earthquakes, while Bouchon et al. (1998a,b) analyzed the 1992 Landers and the 1995 Hyogo-ken Nanbu (Kobe) earthquakes, respectively.

Having computed the spatio-temporal evolution of stress changes over the fault plane, Bouchon (1997) selected to plot three measures of stress change over the fault plane: (1) the strength excess; (2) the dynamic stress drop; (3) the static stress drop. The next step would be to identify the regions of the fault plane responsible for the radiation of the intense near-fault velocity pulses. For example, Wald et al. (1996), in their slip inversion analysis of the 1994 Northridge earthquake, attempted this task by trial-and-error (see their Figure 17). We proposed to relate the slip distribution and the above measures of stress change to the near-fault velocity pulses using the concept of "isochrone" curves. The intention was to explore whether there is a discernible pattern in the slip and/or stress change distribution that favorably generates a certain waveform. Stating this differently, certain "patches" of large moment release on the fault plane behave either as cracks surrounded by "barriers" or as "asperities" (Aki, 1984).

We have developed a computer code implementing the "Discrete Wave-number Method" discussed above. The events that we analyzed are: (1) The 1979 Imperial Valley, California, earthquake (FIGURE 1); (2) the 1989 Loma Prieta, California, earthquake (FIGURE 2); (3) the 1985 Michoacan, Mexico, earthquake (FIGURE 3); and (4) the 1999 Izmit, Turkey, earthquake (FIGURE 4). [In the proposal we had proposed to analyze the 1999 Chi-Chi, Taiwan earthquake, and re-analyze the 1994 Northridge, California earthquake using the inversion solution of Hartzell et al. (1996) who considered also the high-frequency radiation; Bouchon (1997) had already analyzed this event using the inversion results of Wald et al. (1996). We considered

however that it would more productive to analyze the 1985 Michoacan earthquake, instead of the 1999 Chi-Chi earthquake, in view of the fact that the rupture of the former event was simpler and more representative of a major subduction zone event. Similarly, we decided to analyze the 1999 Izmit earthquake instead of the 1994 Northridge earthquake, as representative of a major event on a transform fault such as the North Anatolian fault or the San Andreas fault.]

Analysis of the 1979 Imperial Valley that has already been analyzed by Bouchon (1997), serves as validation exercise for the computer code that we have developed. The 1989 Loma Prieta earthquake also has been previously analyzed by Bouchon (1997). However, Bouchon (1997) used the inversion calculated by Beroza (1991), while we used the inversion developed by Zeng et al. (1993), which is based on higher frequency data and thus reflects a higher resolution of the fault processes on the fault plane. On the other hand, the state of stress on the fault planes of the 1985 Michoacan and 1999 Izmit earthquakes are computed for the first time.

FIGURE 5 displays three *measures of stress change* over the fault plane that are of interest: (1) the *strength excess* (the strength increase at the onset of the rupture denotes the strength excess that when added to the initial stress gives the yield stress of the rock to rupture); (2) the *dynamic stress drop* (corresponds to the largest drop from the initial shear stress level during the rupture process); (3) the *static stress drop* (measures the change in stress produced by the earthquake).

FIGURES 6, 7, 8, & 9 display the abovementioned three measures of stress change for the four events under investigation. The following observations can be made:

- The distributions of strength excess, dynamic stress drop, and static stress drop over the earthquake fault are characterized by large heterogeneity. This is an indication that both the pre-earthquake shear stress and the fault strength vary considerably over the fault plane.
- The slip and stress drop distributions on the fault are strongly correlated; that is, regions where high stress drop occurs coincide with regions where large slip takes place. This observation indicates that large slip is locally driven by high stress drop.
- Comparison of the dynamic and static stress drop images indicates that both spatial distributions follow the same variation pattern. As anticipated, the dynamic stress drop is higher than the static stress drop by a percentage that varies over the fault plane.
- A negative static stress drop value implies a higher level of shear stress after the earthquake. The white areas in the top images of FIGURES 6 and 8 indicate regions of the earthquake faults that exhibited a shear-stress increase. These areas coincide with low slip regions of the fault plane. In addition, it should be pointed out that the highest stress increases take place at the margins of the high slip patches.
- High aftershock seismic activity (not shown here) tends to be concentrated in regions characterized by negative stress drop values. In these areas of the fault, the stress increase during the mainshock has brought the post-earthquake stress level closer to the yield strength (and therefore the specific area of the fault closer to rupture).
- High foreshock seismic activity tends to be concentrated in regions characterized by a pre-earthquake stress level very close to the yield strength (or static friction). As a result, in these areas, the strength excess associated with the mainshock is low.
- A high strength excess value implies that either the fault strength was high or the shear stress was low at that specific area of the fault prior the earthquake.
- The spatial distribution of the strength excess over the fault plane appears to be inversely correlated to the local rupture velocity; that is, low rupture velocity implies high strength excess, while high rupture velocity implies low strength excess [e.g., Day (1982), Quin

(1990)]. This feature was particularly noticeable in the 1979 Imperial Valley earthquake characterized by large variability in rupture velocity (i.e., ranging from subshear to supershear).

- The variation of the shear stress close to the fault edges is not always reliable due to discontinuities in the fault slip (i.e., slip goes from a finite value on the fault plane to a null value outside the fault).
- The resolution of the shear-stress images is of the order of 2 to 3 km comparable to the resolution of the kinematic slip models exploited in the computation of stresses [this resolution may be higher for the 1989 Loma Prieta earthquake model (~ 1 to 2 km) for the reasons that we mentioned earlier]. This implies that short scale-length features of the slip variation remain unresolved. Therefore, it is possible that the high degree of heterogeneity that characterizes the stress distributions over the fault plane may exist at finer scales as well. Moreover, this observation suggests that the stress drops inferred using the methodology of Bouchon (1997) may be regarded as a lower bound to the actual stress drop values.
- The values of strength excess and dynamic stress drop obtained from the shear-stress time histories are sensitive to the maximum frequency considered in the stress computations. In order to get stable values of these two parameters, the simulations should be carried out to higher frequencies (e.g., 5 Hz or lager).

In order to relate the slip distribution and the above measures of stress change to the near-fault velocity pulses we exploit the concept of "*isochrone*" curves. Isochrone is the *locus* of all those points on the fault plane the radiation of which arrives at a certain observer at a specified time. A different set of isochrones corresponds to each station.

In order to make the contrast more stark, we compare the results of the smallest, in size, event (1979 Imperial Valley, M_w 6.5) with those of the largest (1985 Michoacan, M_w 8.1). FIGURES 10 & 11 display the results for the small (M_w 6.5) and large (M_w 8.1) events, respectively. Focusing first on the small event (FIGURE 10), we observe that: (1) Seismic energy radiated from the *high-isochrone-velocity region* of the fault arrives at the receiver within a time interval that coincides with the time window of the ground motion pulse recorded at the site; (2) near-fault strong motion pulses are strongly correlated with *large slip* on the fault plane locally driven by *high stress drop*; and (3) for smaller earthquakes (such as the 1979 Imperial Valley earthquake), the area of the fault that contributes to the formation of the near-fault pulse encompasses more than one "*patches*" of significant moment release (*subevents*). The last observation should be contrasted with what is observed in FIGURE 11 for the very large event. Specifically, in FIGURE 11 we observe that the area of the fault that contributes to the formation of the near fault pulse for a major event (such as the 1985 Michoacan earthquake) encompasses an individual "*patch*" of significant moment release (subevent). This explains why a dislocation model with average properties (i.e., average slip, rise time, etc) reproduces reasonably well near-fault motions for events such as the 1979 Imperial Valley earthquake (Aki, 1979), while a crack model would be necessary to model the near-fault motions of a mega-thrust event such as the 1985 Michoacan earthquake (Yomogida, 1988).

Task 2:

We follow Bouchon and Aki (1982) in simulating time histories of the dynamic deformation field (i.e., strain, rocking, and torsion) in the vicinity of faults embedded in a layered half-space using the discrete wavenumber representation method (Bouchon and Aki, 1977; Bouchon, 1979). A sample of the results is shown in FIGURE 12 which displays various

components of the deformation field for the 1979 Imperial Valley earthquake. The following observation can be made (these observations / conclusions are valid also for the other events):

- The simulation results satisfy equations $(\partial u_x/\partial z) = -(\partial u_z/\partial x)$ and $(\partial u_y/\partial z) = -(\partial u_z/\partial y)$ which follow from the stress-free boundary condition at the free surface of the Earth [we consider a right-handed Cartesian system of coordinates in which x- & y- are the horizontal axes, and z- is the vertical axis; furthermore, the x-axis is *parallel* to the *strike* of the fault (*fault-parallel* component), while the y-axis is normal to it (*fault-parallel* component)]. In addition, the approximation of Equation $\omega_z = (1/2)(\partial u_y/\partial x - \partial u_x/\partial y) \approx (1/2)(\partial u_y/\partial x)$ appears to be reasonably accurate for most near-fault stations.
- The axial strains are characterized by relatively small amplitudes with the exception of strains in the transverse direction (i.e., $\partial u_y/\partial y$) for stations located very close to the causative fault. Furthermore, the results illustrate that extension in one horizontal direction is associated with compression in the other horizontal direction.
- The amplitudes of the torsional components of the dynamic deformation field are larger than the amplitudes of the respective rocking components. Furthermore, rocking along the strike-parallel direction is consistently larger than rocking along the strike-normal direction. These observations are in agreement with estimates of actual rotational components of seismic waves inferred using data from the SMART-1 strong motion array in Taiwan (Oliveira and Bolt, 1989).
- Torsion and rocking components of ground motion obtained along a transverse profile to the fault trace reveal that peak rotations decrease quite rapidly with distance to the fault. This observation becomes more apparent if results of additional receiver points, not shown in FIGURE 12, are also considered. As explained by Bouchon and Aki (1982), the attenuation characteristics primarily depend on the type of waves present.
- The simulation results indicate that the peak values of rocking and torsion at the stations depicted in FIGURE 12 were of the order of 10^{-4} rad. These values are in good agreement with estimates of ground rotations available in the literature based on actual strong motion data. For instance, the peak rotation amplitudes estimated by Niazi (1986) from analysis of the three components of recorded accelerations along the El Centro linear differential array during the 1979 Imperial Valley earthquake were in the range of 10^{-4} to $3\ 10^{-4}$ rad (when relatively large station distances were considered in the analysis).

The top three panels of FIGURE 12 display the time series of the $\partial u_x/\partial x$, $\partial u_y/\partial x$, and $\partial u_z/\partial x$ components of the deformation tensor (E_{ij}) for selected stations of FIGURE 1. The bottom three panels illustrate the three components of the velocity time histories generated at the same locations. Comparison of these two sets of data reveals a remarkable similarity (at least over the segment of intense ground motion) between the waveforms of the velocity time histories and the derivatives of the displacement components with respect to distance along the fault strike (i.e., x coordinate). This indicates that most of the energy (which controls the peak amplitudes of motion) propagates at each observation point within a relatively small range of phase velocities and thus the relationship

$$\frac{\partial u_i}{\partial x} \approx -\frac{1}{c}\frac{\partial u_i}{\partial t} \qquad (2)$$

(with c being the *average phase velocity*) is approximately valid.

The phase velocities may be estimated from the synthetic time histories of FIGURE 12 using Equation (2). For the depicted stations, the estimated phase velocities turn out to be close to the shear wave velocity of the basement rock (4 to 5 km/s). This observation confirms the proposition that phase velocities are controlled either by the basement rock shear velocity or the rupture velocity, and not by the shear wave velocity of unconsolidated sediments (e.g., Luco and

Sotiropoulos, 1980; Bouchon and Aki, 1982). Since the rupture velocity of the 1979 Imperial Valley earthquake was highly variable, the relationship between phase and rupture velocities for this particular seismic event is rather unclear.

Therefore, the *axial strain* along the strike direction ($\omega_{xx} = \partial u_x/\partial x$), the rocking along the transverse direction ($\omega_y = -\partial u_z/\partial x$), and the torsional motion [$\omega_z \approx 0.5*\partial u_y/\partial x = -(1/2c)*\partial u_y/\partial t = -(1/2c)*V_g$, where V_g is the *fault-normal* component of the ground velocity] may be estimated with reasonable accuracy through Equation (2) by using synthetic (or actual) ground velocities and properly selected phase velocities. It is evident that the analytical model proposed in Equation 1 for the replication of the long-period (coherent) component of the near-fault ground motion (along with properly selected phase velocities) may be exploited in a straightforward manner to approximate the torsional component of the near fault ground motion both in qualitative and quantitative terms. This development facilitates the parametric investigation of the dynamic response of structures susceptible to torsional motions as a function of the input parameters of the ground motion mathematical model.

Task 3:

We have investigated the response of structures to the translational and torsional motions induced in the near-fault region. In order to assess the soundness of existing code provisions, we investigated the response to simple near-fault pulses of a relatively simple structural model (FIGURE 13) that has been proposed by Luco (1976). The model consists of a cylindrical shaft that responds to translational motion as a "*shear beam*". The shaft is supported on a circular rigid foundation, which, in turn, is supported on an elastic half-space. The frequency characteristics of the input and of the structural response, along with the transfer function of the structure, are shown in FIGURE 14. An example of the time-domain response of the structural model to near-fault pulses (as described by Equation 1) is shown in FIGURE 15. In order to assess the necessary accidental eccentricity e to account for the torsional response due to "near-fault" motions, we make use of the following expression which is based on Newmark's (1969) original analysis:

$$\frac{e}{2a} = \left(\frac{\sqrt{2}}{4}\right)\cdot\left(\tilde{u}_0 - 1\right)\cdot\left(\frac{\omega_\theta}{\omega_y}\right)^2 \qquad (3)$$

where: a is the radius of the circular foundation, $\tilde{u}_0 = (u_{T0}/u_x)$ is the ratio of the total (i.e. torsional + translational) response to the translational response, and ω_θ and ω_y are the characteristic (fundamental) circular frequencies of the structure to torsion and translation. In FIGURE 16, the normalized accidental eccentricity ($e/2a$) is plotted as a function of the normalized phase velocity a_1. Although the normalized accidental eccentricity may take large values, depending on the values of the various parameters of the problem, for realistic values of the parameters (and in particular of the parameter a_1 which represents the normalized *apparent surface velocity*) the eccentricity ($e/2a$) does not exceed 5%, which is the value imposed by the building code. The reason for this is that the excitation in Equation (3) enters in the form of a ratio, i.e. $\tilde{u}_0 = (u_{T0}/u_x)$, and consequently, no matter how intense are the near-fault pulses, the ratio remains stable. Therefore, we conclude that the current provisions of the code regarding torsional response to near-fault motions are adequate and in fact conservative.

Finally, we have also developed a mathematical model to represent the tower of a cable-stayed bridge that accounts for soil-structure-interaction. We are currently in the process of performing parametric studies of the response of the structural model to near-fault motions.

REFERENCES

Aki, K. (1979). Evolution of quantitative models of earthquakes, in *Fracture Mechanics*, R. Burridge (Editor), *SIAM-AMS Proceedings* **12**, 43-58.

Aki, K. (1984). Asperities, barriers, characteristic earthquakes and strong motion prediction, *J. Geophys. Res.* **89**, 5867-5872.

Archuleta, R. J. (1984). A faulting model for the 1979 Imperial Valley earthquake, *J. Geophys. Res.* **89**, 4559-4585.

Beroza, G. C. (1991). Near-source modeling of the Loma Prieta earthquake: Evidence for heterogeneous slip and implications for earthquake hazard, *Bull. Seism. Soc. Am.* **81**, 1603-1621.

Bouchon, M. (1979). Discrete wave-number representation of elastic wave fields in three-space dimensions, *J. Geophys. Res.* **84**, 3609-3614.

Bouchon, M. (1997). The state of stress on some faults of the San Andreas system as inferred from near-field strong motion data, *J. Geophys. Res.* **102**, 11731-11744.

Bouchon, M., and K. Aki (1977). Discrete wave-number representation of seismic-source wave fields, *Bull. Seism. Soc. Am.* **67**, 259-277.

Bouchon, M., and K. Aki (1982). Strain, tilt, and rotation associated with strong ground motion in the vicinity of earthquake faults, *Bull. Seism. Soc. Am.* **72**, 1717-1738.

Bouchon, M., M. Campillo, and F. Cotton (1998a). Stress field associated with the rupture of the 1992 Landers, California, earthquake and its implications concerning the fault strength as the onset of the earthquake, *J. Geophys. Res.* **103**, 21091-21097.

Bouchon, M., H. Sekiguchi, K. Irikura, and T. Iwata (1998b). Some characteristics of the stress field of the 1995 Hyogo-ken (Kobe) earthquake, *J. Geophys. Res.* **103**, 24271-24282.

Bouchon, M., M. N. Töksoz, H. Karabulut, M.-P. Bouin, M. Dietrich, M. Aktar, and M. Edie (2002). Space and time evolution of rupture and faulting during the 1999 Izmit (Turkey) earthquake, *Bull. Seism. Soc. Am.* **92**, 256-266.

Day, S. M. (1982). Three-dimensional simulation of spontaneous rupture: The effect of nonuniform prestress, *Bull. Seism. Soc. Am.* **72**, 1881-1902.

Hartzell, S., P. Liu, and C. Mendoza (1996). The 1994 Northridge, California, earthquake: Investigation of rupture velocity, rise time, and high-frequency radiation, *J. Geophys. Res.* **101**, 20091-20108.

Luco, J. E. (1976). Torsional response of structures to obliquely incident seismic *SH* waves, *Earthquake Engrg. Struct. Dyn.* **4**, 207-219.

Luco, J. E., and D. A. Sotiropoulos (1980). Local characterization of free-field ground motion and effects of wave passage, *Bull. Seism. Soc. Am.* **70**, 2229-2244.

Mavroeidis, G. and A.S. Papageorgiou (2002a). "The Characteristics of Near-field Ground Motions & Their Implications on Seismic Response of Suspension Bridges", *Proceedings of the Third National Seismic Conference & Workshop on Bridges & Highways*, Portland, Oregon, April 28 – May 1, 2002, pp. 533-537.

Mavroeidis, G.P., and A.S. Papageorgiou (2002b). Near-source strong ground motion: Characteristics and design issues. *Proceedings of the 7th U.S. National Conference on Earthquake Engineering*, Boston, Massachusetts, July 21-25, 2002.

Mavroeidis, G. P., and A. S. Papageorgiou (2003). A mathematical representation of near-fault ground motions, *Bull. Seism. Soc. Am.* **93**, 1099-1131.

Mavroeidis, G., G. Dong, and A.S. Papageorgiou (2004). "Near-Fault Ground Motions, and the Response of Elastic and Inelastic Single-Degree-of-Freedom (SDOF) Systems", *Earthquake Engineering and Structural Dynamics*, Vol. **33**, pp. 1023-1049.

Mendoza, C., and S. H. Hartzell (1989), Slip distribution of the 19 September 1985 Michoacan, Mexico, earthquake: Near-source and teleseismic constraints, *Bull. Seism. Soc. Am.* **79**, 655-669.

Newmark, N. M. (1969). Torsion in symmetrical buildings, in *Proc. of the Fourth World Conference on Earthquake Engineering (4WCEE)*, Santiago, Chile.

Niazi, M. (1986). Inferred displacements, velocities and rotations of a long rigid foundation located at El Centro differential array site during the 1979 Imperial Valley, California, earthquake, *Earthquake Engrg. Struct. Dyn.* **14**, 531-542.

Oliveira, C. S., and B. A. Bolt (1989). Rotational components of surface strong ground motion, *Earthquake Engrg. Struct. Dyn.* **18**, 517-526.

Quin, H. (1990). Dynamic stress drop and rupture dynamics of the October 15, 1979 Imperial Valley, California, earthquake, *Tectonophysics* **175**, 93-117.

Wald, D. J., T. H. Heaton, and K. W. Hudnut (1996). The slip history of the 1994 Northridge, California, earthquake determined from strong-motion, teleseismic, GPS, and leveling data, *Bull. Seism. Soc. Am.* **86**, S49-S70.

Yomogida, K. (1988). Crack-like rupture process observed in near-fault strong motion data, *Geophys. Res. Lett.* **15**, 1223-1226.

Zeng, Y., K. Aki, and T.-L. Teng (1993b). Mapping of the high-frequency source radiation for the Loma Prieta earthquake, California, *J. Geophys. Res.* **98**, 11981-11993.

FIGURES

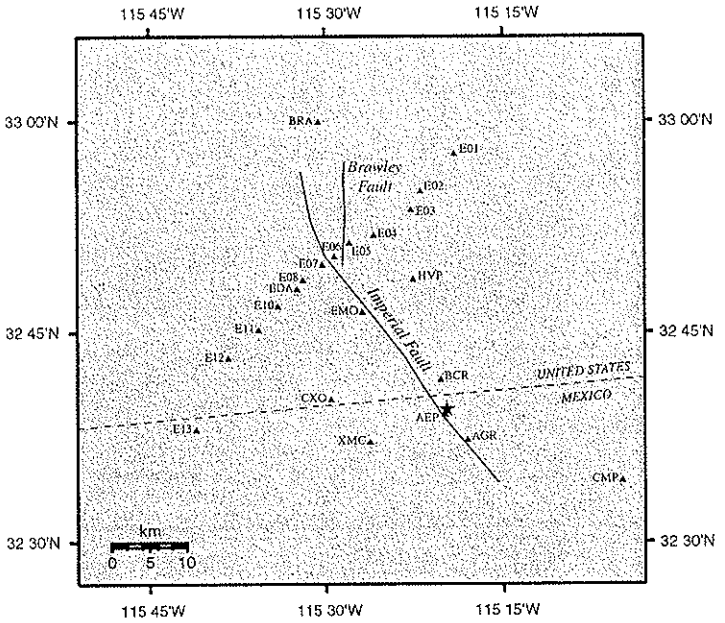

FIGURE 1: Map view of the Imperial Valley area showing locations of accelerographs, the Imperial and Brawley faults, the location of the epicenter, and the United States-Mexico border.

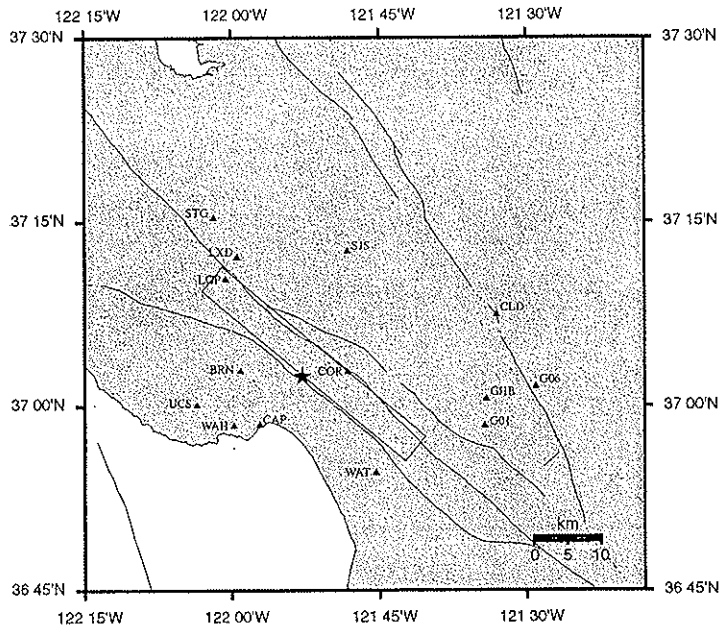

FIGURE 2: Map view of the epicentral region of the 1989 Loma Prieta earthquake showing the location of the epicenter, the projection of the idealized fault plane on the free surface, locations of accelerographs, and mapped faults in the area.

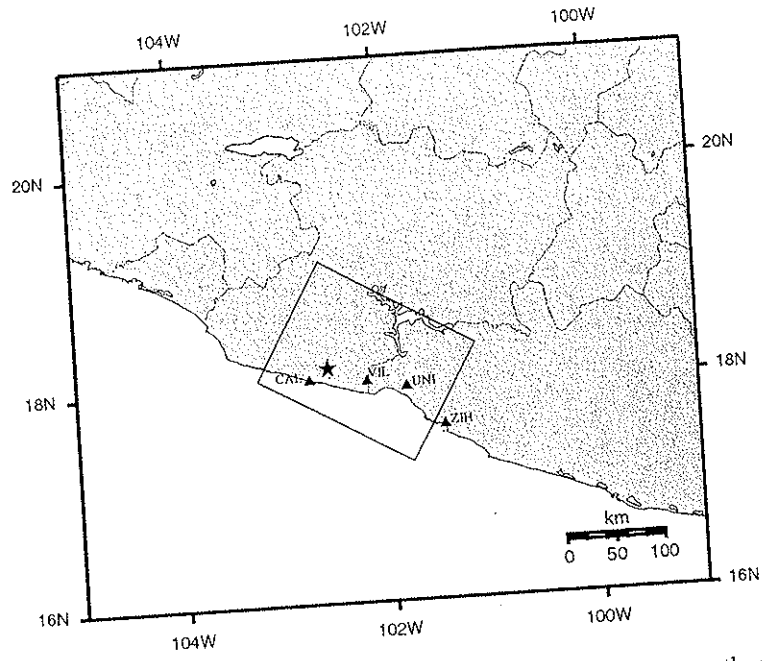

FIGURE 3: Map view of the epicentral region of the 1985 Michoacan earthquake showing the location of the epicenter, the projection of the idealized fault plane on the free surface, and locations of accelerographs.

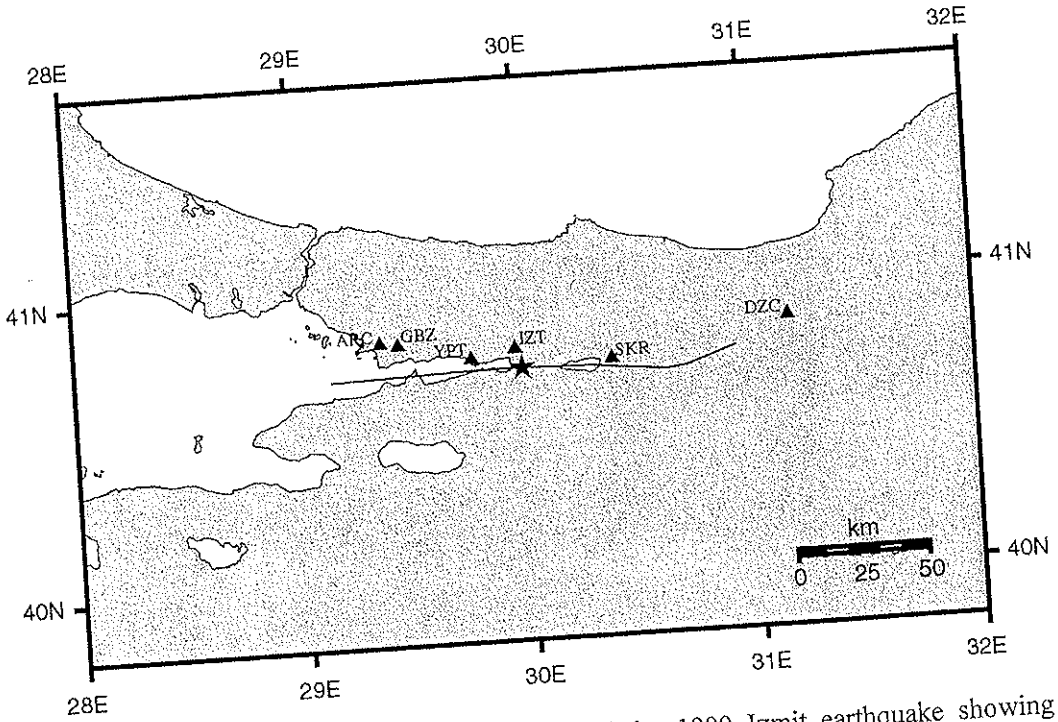

FIGURE 4: Map view of the epicentral region of the 1999 Izmit earthquake showing the location of the epicenter, the projection of the idealized fault on the free surface, and locations of accelerographs.

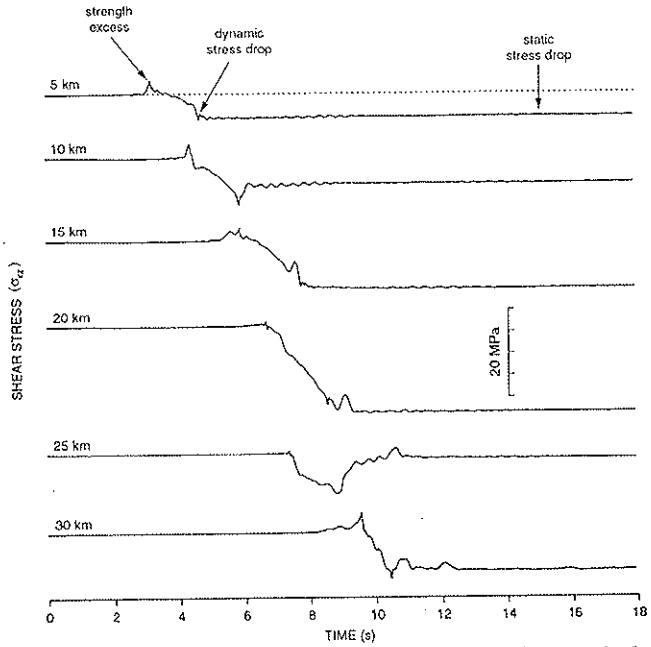

FIGURE 5: Time histories of shear stress along the strike direction at six locations on the Imperial Fault during the 1979 Imperial Valley earthquake. Numbers on the left indicate epicentral distances. The down-dip distance considered is 10 km.

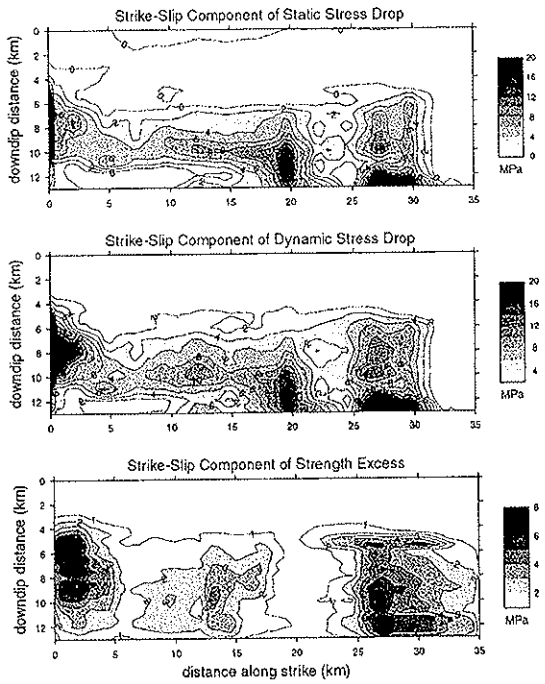

FIGURE 6: Spatial distribution of static stress drop (top), dynamic stress drop (middle), and strength excess (bottom) on the Imperial Fault based on the rupture model inferred by Archuleta (1984).

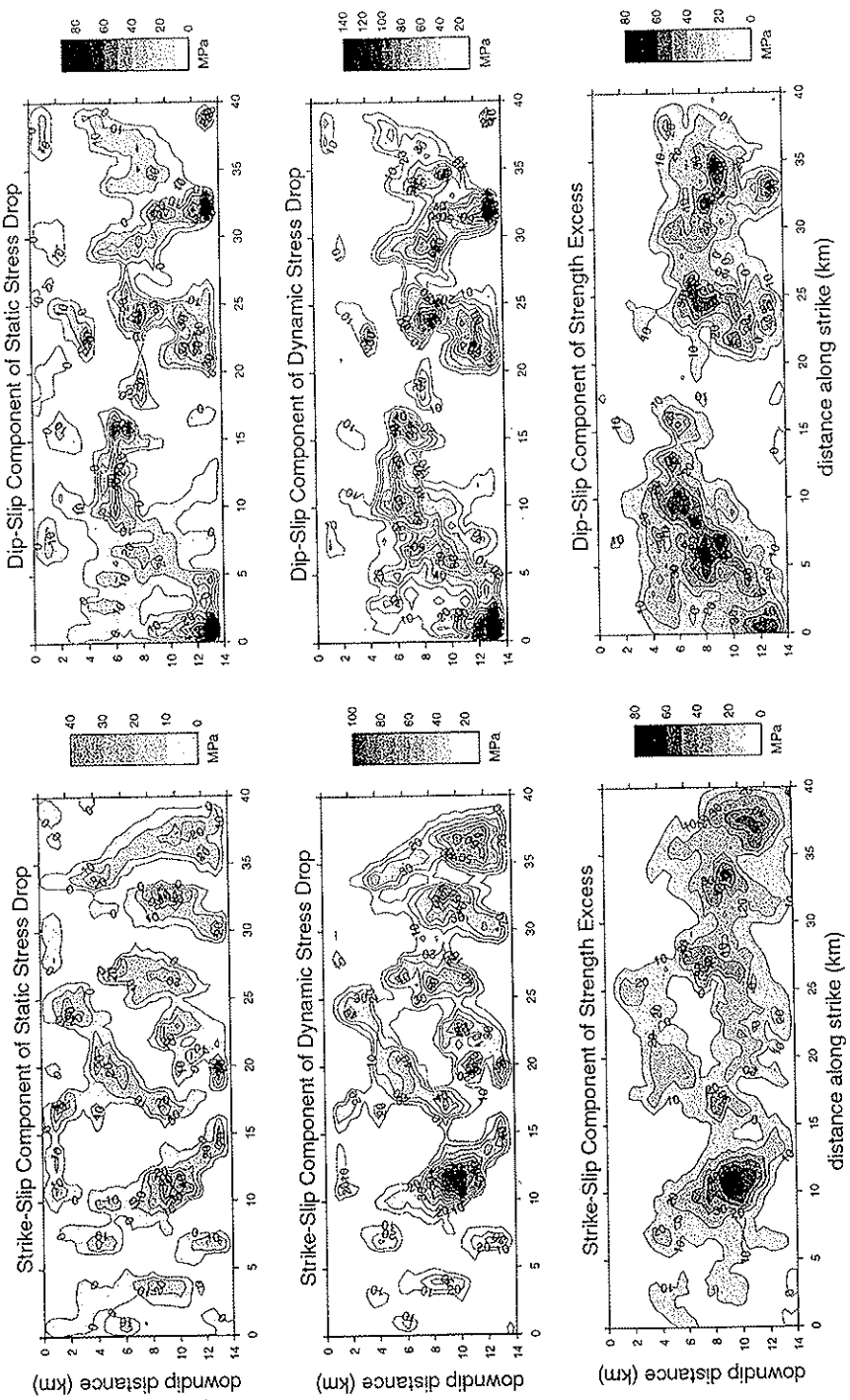

FIGURE 7: Spatial distribution of static stress drop, dynamic stress drop, and strength excess along strike and dip on the causative fault of the 1989 Loma Prieta earthquake based on the fault model inferred by Zeng et al. (1993).

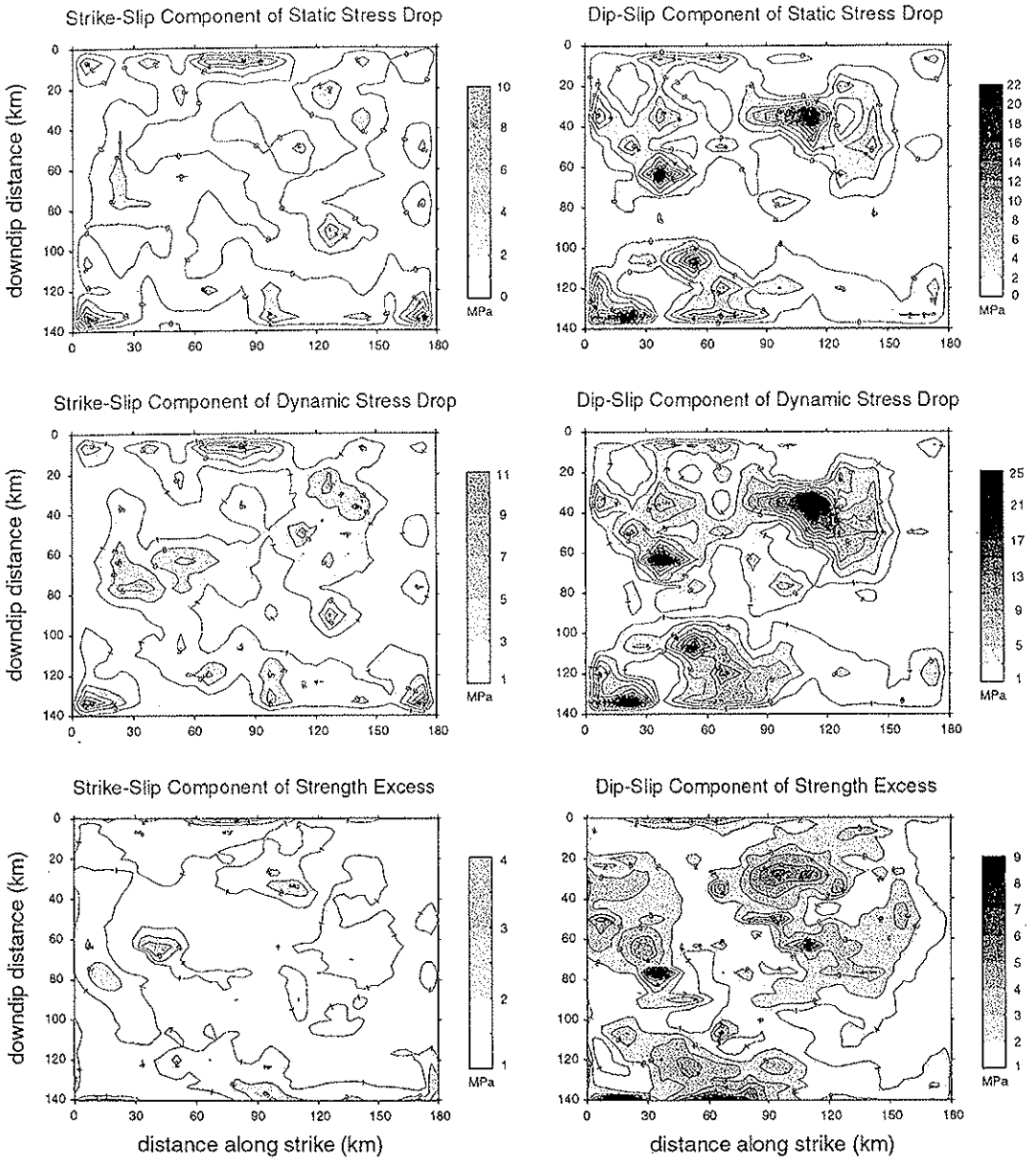

FIGURE 8: Spatial distribution of static stress drop, dynamic stress drop, and strength excess along strike and dip on the causative fault of the 1985 Michoacan earthquake based on the fault model inferred by Mendoza and Hartzell (1989).

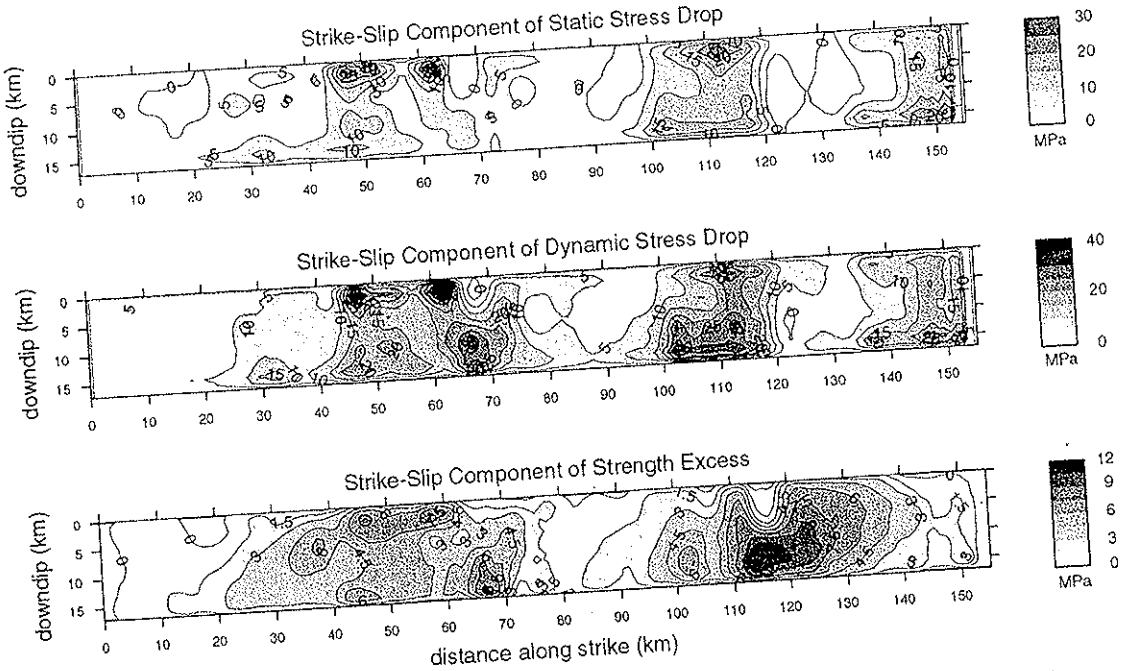

FIGURE 9: Spatial distribution of static stress drop (top), dynamic stress drop (middle), and strength excess (bottom) on the causative fault of the 1999 Izmit earthquake based on the fault model inferred by Bouchon et al. (2002).

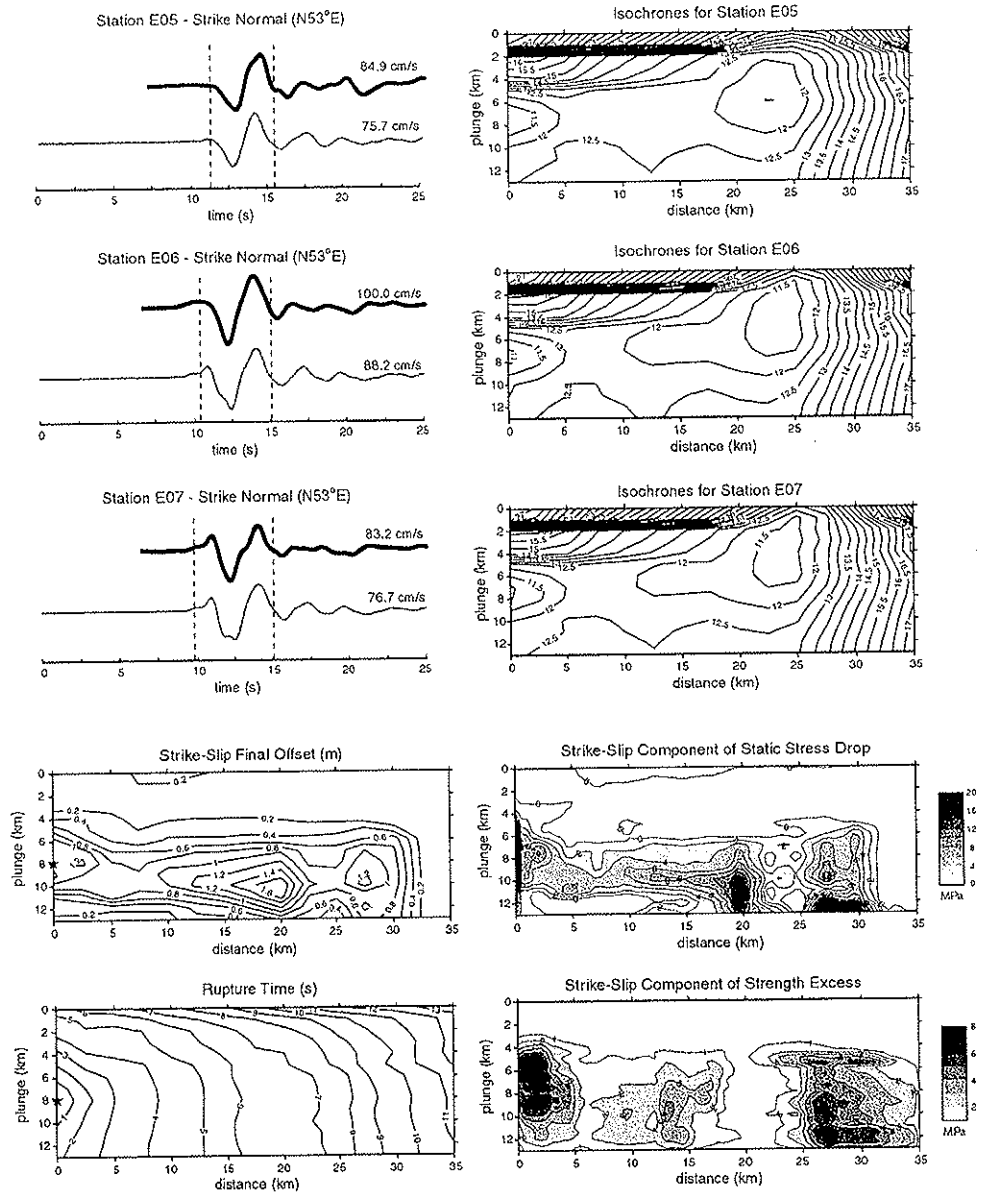

FIGURE 10: Recorded (black trace) and synthetic (gray trace) near-fault ground motion time histories and *S*-wave isochrones for selected stations of the 1979 Imperial Valley earthquake. Tomographic images of the static slip offset, rupture time, static stress drop, and strength excess are also illustrated.

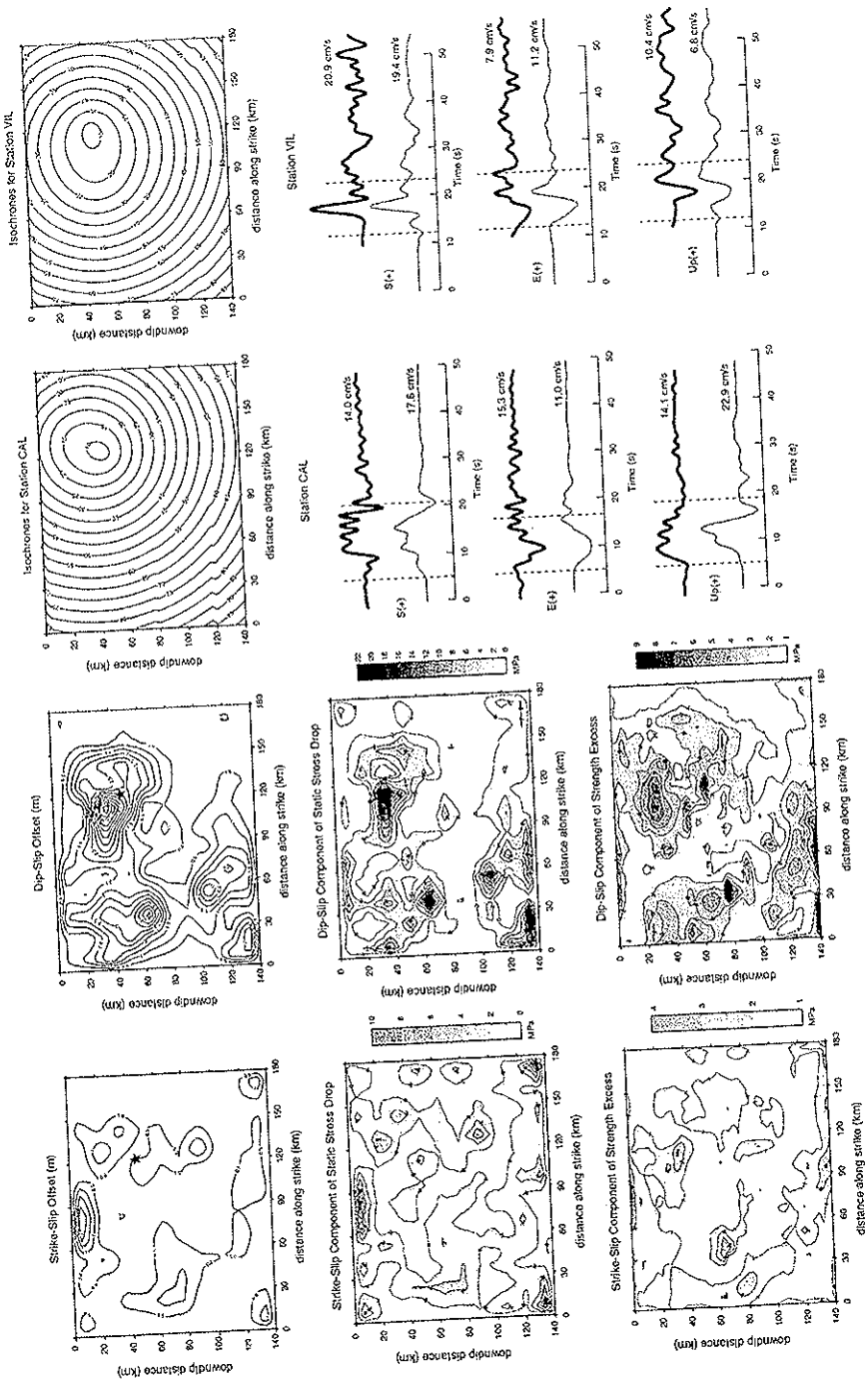

FIGURE 11: Recorded (black trace) and synthetic (gray trace) near-fault ground motion time histories and *S*-wave isochrones for stations of the 1985 Michoacan earthquake. Tomographic images of the static slip offset, static stress drop, and strength excess along the strike and dip directions are also illustrated.

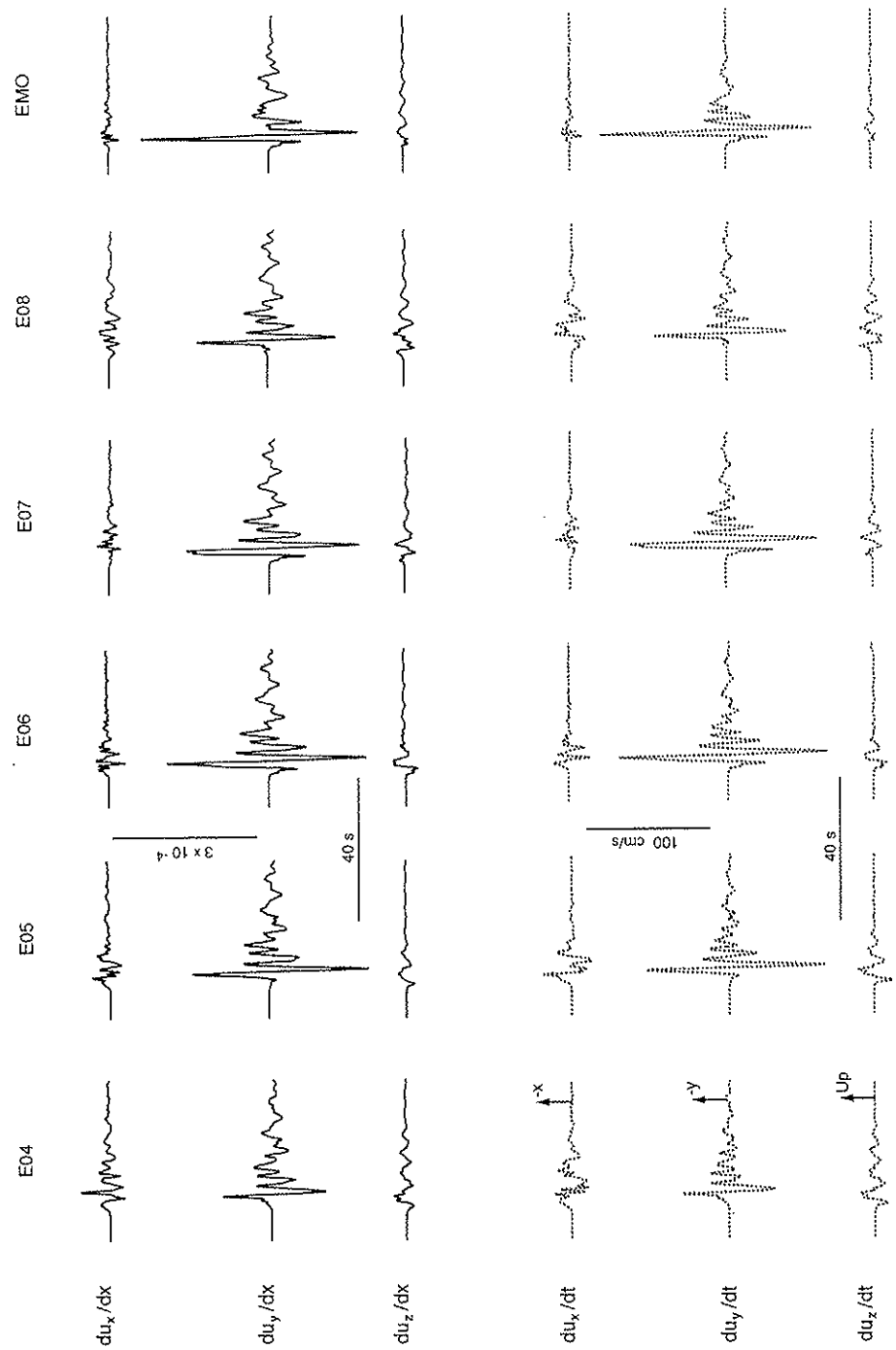

FIGURE 12: Comparison between time series of specific components of the deformation tensor (i.e., $\partial u_i/\partial x$, i=x, y, z) and time histories of the ground velocity components (i.e., $\partial u_i/\partial t$, i=x, y, z) for selected stations of the 1979 Imperial Valley earthquake.

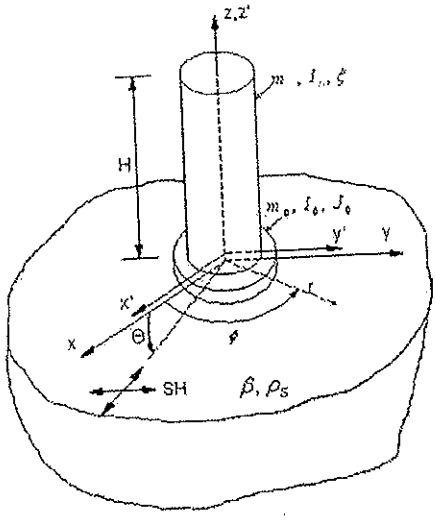

FIGURE 13: Structural model proposed by Luco (1976). The model consists of a cylindrical shaft that responds to translational motion as a "*shear beam*". The shaft is supported on a circular rigid foundation, which, in turn, is supported on an elastic half-space.

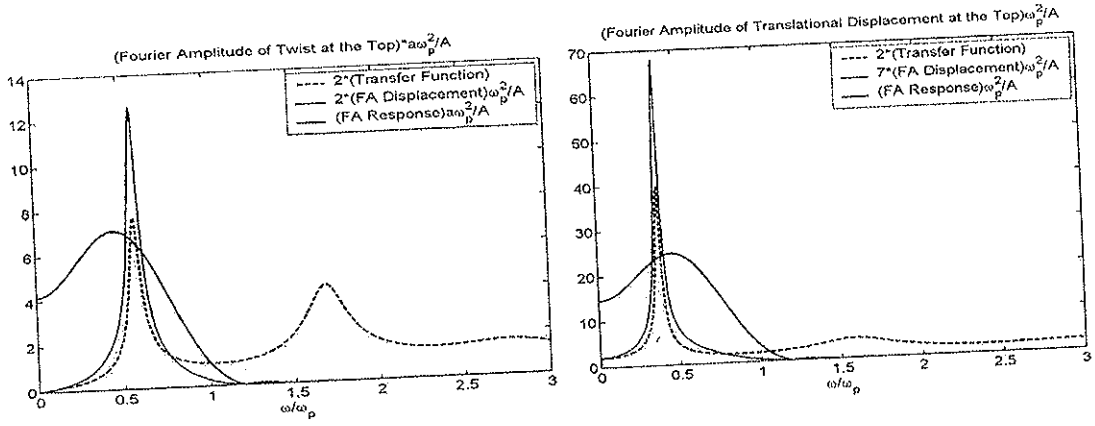

FIGURE 14: Fourier amplitude spectra of the excitation (near-fault pulse) and of the response (twist and translational displacement) at the top of the structural model. The transfer function of the structural model is indicated by the dashed line.

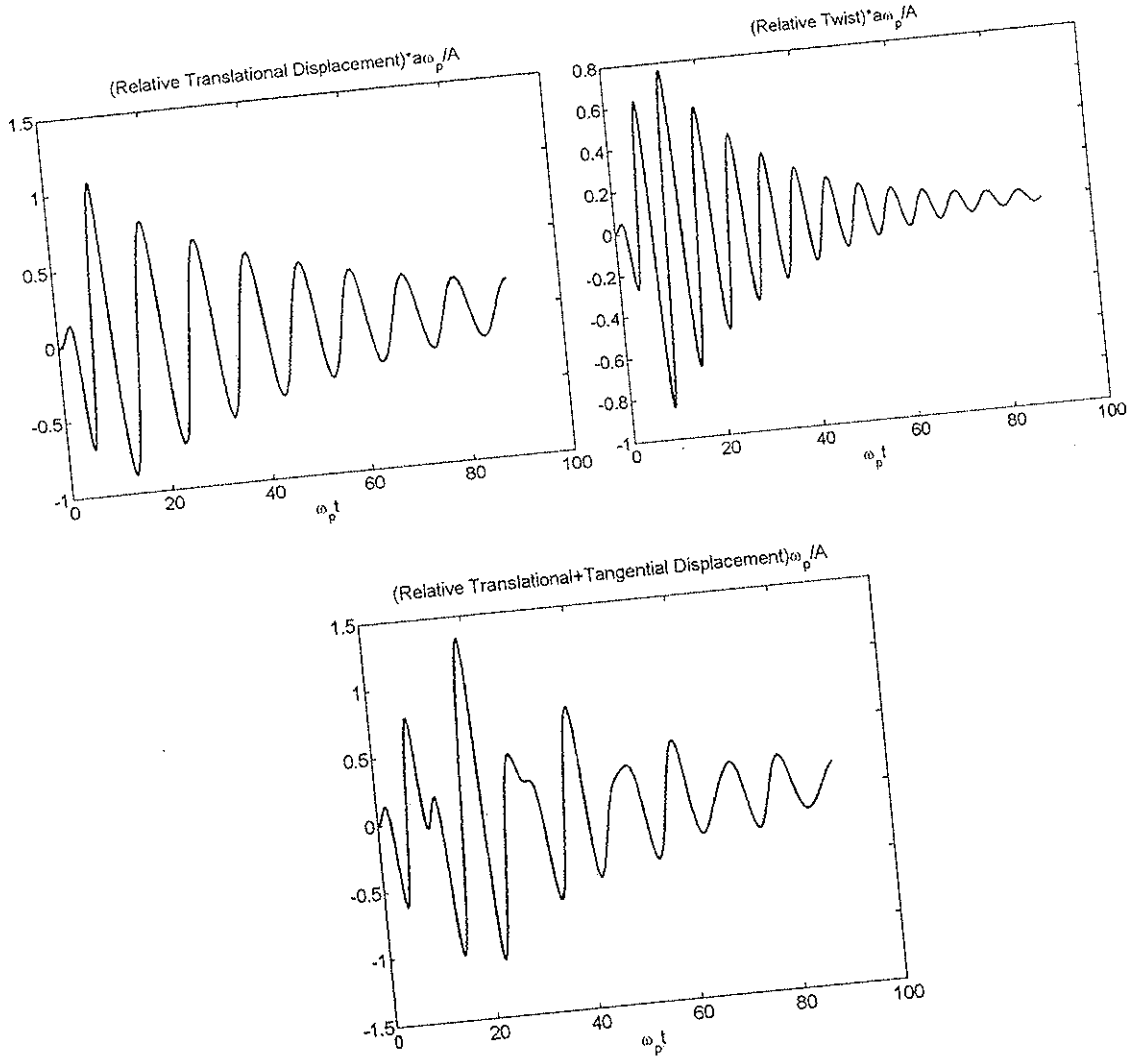

FIGURE 15: Translational and torsional (twist) displacement at the top of the structural model relative to the base / foundation.

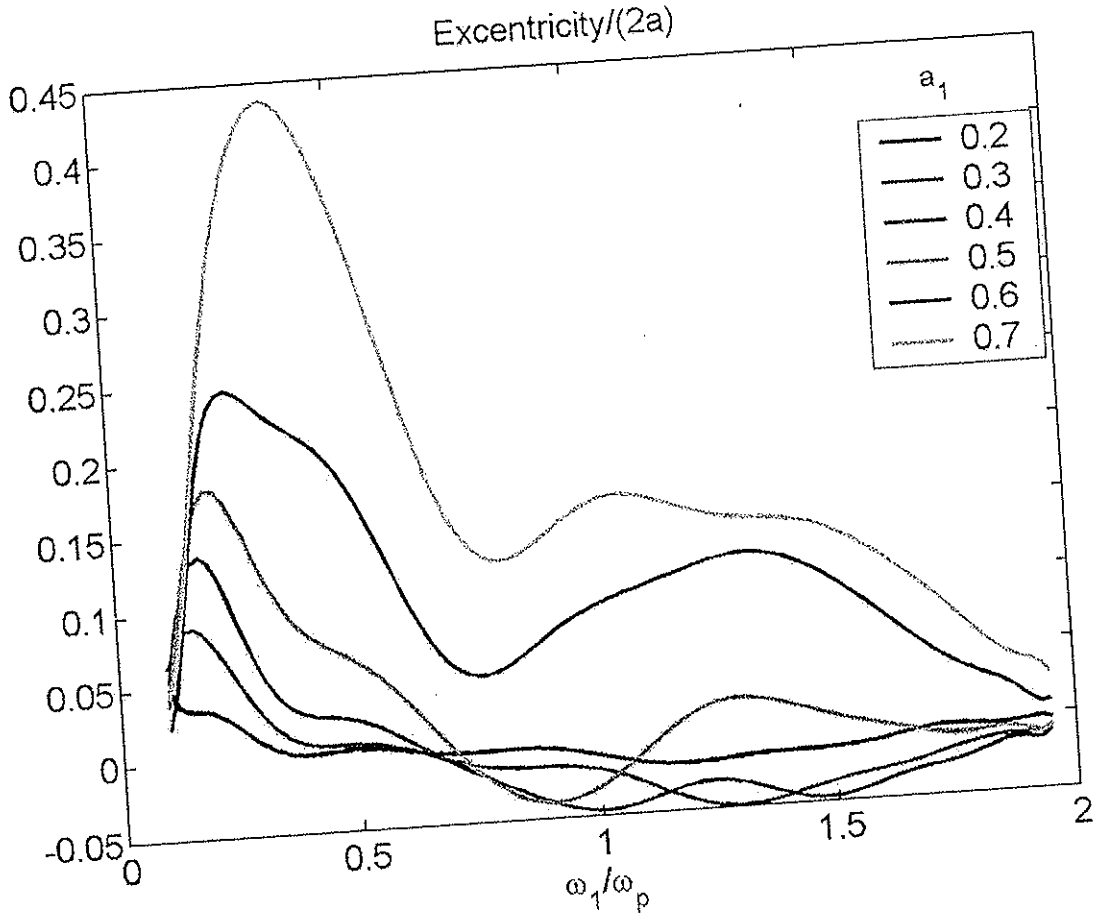

FIGURE 16: *Normalized accidental eccentricity* ($e/2a$) as a function of normalized frequency and for various values of the *apparent surface velocity* a_1.

PUBLICATIONS THAT RESULTED FROM THE WORK PERFORMED DURING THE 12-MONTH PERIOD OF THE RESEARCH PROJECT

Meza-Fajardo, K.-C. and A.S. Papageorgiou (2004). "Torsional Response of Structures to Impulsive Near-fault Ground Motions", ***Seismological Research Letters***, Vol. **74**, No. **2**, pp.267.

Mavroeidis, G. and A.S. Papageorgiou (2004). "Design Spectra of the Single-Degree-of-Freedom System Subjected to Near-fault Strong Ground Motions", ***Seismological Research Letters***, Vol. **74**, No. **2**, pp. 266.

Mavroeidis, G. and A.S. Papageorgiou (2005). "Effect of Fault Rupture Characteristics on Near-Fault Strong Ground Motions", ***Seismological Research Letters***, Vol. **76**, No. **2**, pp. 247.